INSTRUMENTATION

SPECT Resolution and Uniformity Improvements by Noncircular Orbit

Stephen C. Gottschalk, David Salem, Chun Bin Lim, and Robert H. Wake

Technicare Corporation, Solon, Ohio

A noncircular orbit implemented by a combination of rotational and translational motions in single photon emission computed tomography improves significantly the image resolution and uniformity. The former is realized by closer access of the detector to the object at each projection angle, and the latter by suppression of ring artifacts through the shifts in the distance between the centers of detector and object. This has been demonstrated by comparing the SPECT images for an elliptical orbit of 40 cm × 30 cm with the equivalent circular orbit of 40 cm diameter, performed by SPECT system with a high resolution collimator. Resolution FWHM improvements were 1.5–2.5 mm. Lesion contrast improved by a factor of 2.8 for a nonradioactive rod of 6 mm diam. In phantom images, the elliptical orbit showed better definition of lesion shape, sharper edge response, and clearly increased detectability. Translational motion reduced ring artifacts, particularly near the image center.

J Nucl Med 24: 822–828, 1983

This paper describes experimental results on the image resolution and uniformity improvement in single photon emission computed tomography (SPECT) with a noncircular detector orbit, implemented by a combination of rotational and translational motions, compared with a circular orbit.

Earlier simulations performed by us (*1*) indicated that a noncircular detector orbit achieved by the above motions would give significantly improved resolution and uniformity. The resolution improvement occurs because the detector is brought closer to the patient with respect to the depth-dependent collimator resolution. The uniformity improvement is due to the shifting of the detector center relative to the object center as the detector is rotated, which results in smearing of central-ring artifacts. This shift results from the translational component of the motion.

SPECT resolution is fundamentally limited by the planar projection resolution, which is determined largely by the collimator resolution. Narrowing the gap between detector and patient improves the projection resolution. This results in better SPECT resolution and contrast (*2,3*). We will see that this improves detection of small lesions and gives better edge definition with large lesions.

In SPECT imaging with a circular orbit, the systematic nonuniformity of projection sensitivity causes ring artifacts (*4,5*). Suppression of rings away from the reconstruction center requires imaging a correction flood that is accurate to the 1–2% level (*4,5*), or smoothing of the projections and the correction flood (*5*). In either case the artifact at the reconstruction center remains. During rotation, translation of the detector to achieve a noncircular orbit results in reduction of the central artifact amplitude by a factor of 20 (*1*).

THEORY

Detector motion. The method of achieving a noncircular orbit by a combination of rotational and translational motions is shown in Fig. 1. For illustration we have chosen an elliptical orbit. The initial detector face is horizontal at line 0. The rotation radius is the minor axis of the ellipse. The detector is rotated to angle θ_1 bringing

Received Jan. 26, 1983; revision accepted Apr. 8, 1983.

For reprints contact: Stephen C. Gottschalk, MS, Technicare Corporation, Solon, Ohio 44139.

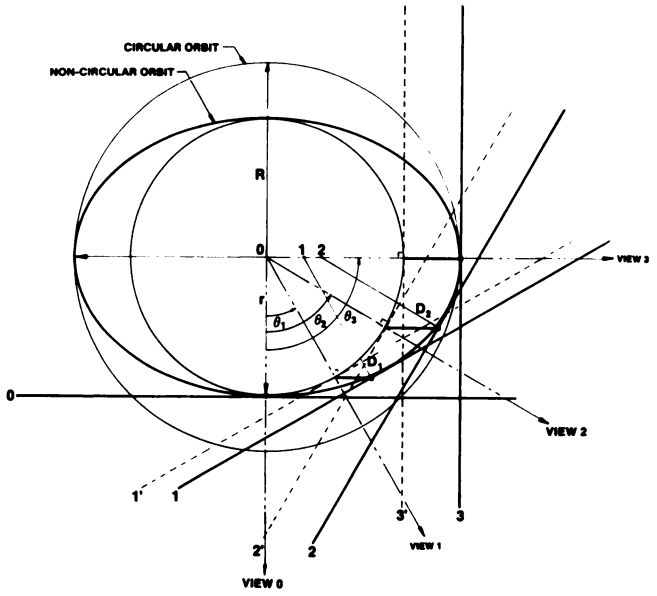

FIG. 1. Schematic of noncircular detector orbit with rotational and translational motion.

the detector surface to the line 1′. Then the detector is translated by an amount D_1 so that its surface 1 becomes tangent to the desired orbit. In general, the point of tangency is not at the center of the detector. The next imaging angle is θ_2. If this were achieved by rotation of θ_2 from the initial horizontal position, then the detector surface would be at line 2′. Then the translation by D_2 would bring the detector to line 2. In practice the detector is rotated from θ_1 to θ_2 and the amount of translation would be $D_2 - D_1$. From the description it is clear that arbitrary orbits can be achieved.

Resolution and contrast. SPECT resolution is a function of the projection resolution, projection bin width, filter used, and the position in the SPECT image (*1–3,6*). The projection resolution depends on the intrinsic detector resolution and that of the collimator. In air, a high resolution (HR) collimator in our system has the resolution (FWHM) shown by the curved line in Fig. 2. The resolution in water is 10–15% poorer. The filter should be chosen to match the detector system's projection MTF, and the projection bin width chosen to minimize aliasing and reduce the effects of sampling. We have chosen a Butterworth filter with a half-power point of $1.1/\mathrm{FWHM_c}$. The $\mathrm{FWHM_c}$ is the projection resolution at the object center. The half-power frequency for the filter was chosen because it produced a resolution that was 0.2 mm worse than that of a ramp filter, but had one third of a ramp's rms noise at the image center. The position-dependence of the SPECT resolution is a consequence of changes in attenuation and collimator resolution with depth.

For the special case of an elliptical orbit, bringing the detector closer for the vertical views will produce improved horizontal resolution. The vertical resolution will remain unchanged. It is clear that the resolution will improve over the entire reconstruction volume, as seen in Fig. 2. The axial component of the 3-D SPECT point spread function (PSF) is determined by the axial projection resolution, which also benefits from a noncircular orbit.

The main sources of contrast degradation in SPECT are the system resolution and scatter-photon contribution. The effect of improving spatial resolution on SPECT lesion contrast is shown in Fig. 3 for a uniform spherical lesion. This was obtained by convolution with the 3-D SPECT PSF. Note the rapid image contrast improvement for small lesions with decreasing FWHM values.

SPECT lesion detectability. Detection of lesions in SPECT imaging depends on the lesion contrast (signal-to-background) relative to the reconstruction photon noise, averaged over a lesion-sized area, divided by the local background level. A requirement that a lesion of given size and contrast be detectable in a circular object with background of uniform activity is provided when

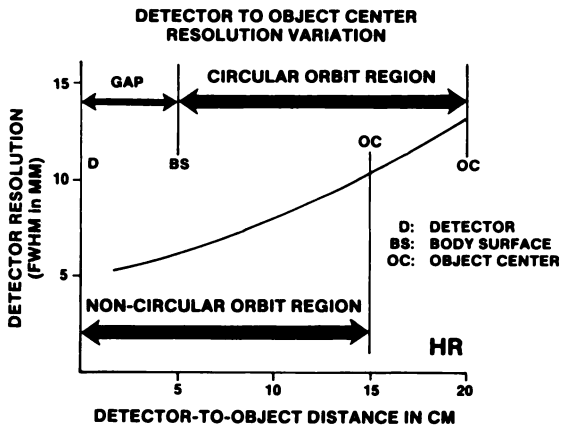

FIG. 2. Resolution range of detector system utilized in noncircular and circular orbits for projection data collection in camera equipped with high-resolution collimator.

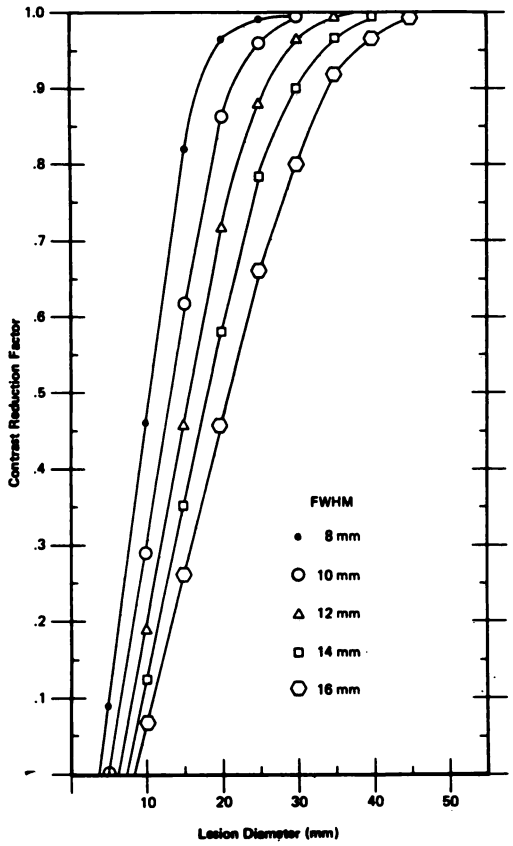

Fig. 3. Improvement of lesion contrast with decrease in system resolution FWHM, calculated by convolution of spherical lesion of uniform activity with Gaussian PSF.

the following inequality is satisfied (3):

$$C_0 \cdot \frac{C_r}{1 + \langle SF \rangle} > k \cdot \frac{b \cdot \left(\frac{D}{d/2}\right)^{3/2}}{\sqrt{N_T}} \cdot f(r)$$

where C_0 = lesion object contrast; d = lesion diameter; D = object diameter; FWHM = system resolution; $C_r(d/FWHM)$ = lesion contrast reduction factor; $\langle SF \rangle$ = average scatter fraction; N_T = total photon counts in a slice; b = noise coefficient, approximately 0.7; f(r) = radial variation of rms noise; and k = threshold S/N ratio of lesion-to-background to guard against statistical false alarm. The C_r (d/FWHM) denotes a function of d and FWHM.

A detectability curve of a spherical lesion in a uniform background 30 cm in diameter is given in Fig. 4, according to the equation, as a function of the lesion size for FWHM = 12.5 mm, <SF> = 60%, k = 4, and N_T = 1 million. The figure also shows the curve for the contrast reduction factor due to spatial resolution. Note the increasing departure of SPECT detectability from the ideal photon-limited case with decreasing lesion size. This is due to finite spatial resolution. Thus resolution improvements lead to better detection of small lesions by narrowing this gap. Improved resolution also aids detection of large lesions by providing sharper edge response coupled with the human psychovisual response. With a decreasing FWHM, the minimum detectable lesion size would decrease for the same photon count, or fewer photon counts would be required for detection of lesions of the same size. These are the mechanisms by which a noncircular orbit allows detection of small and large lesions without increasing the imaging time.

Uniformity. Common SPECT artifacts are rings caused by the systematic nonuniform projection sensitivity. The usual method of compensation is to acquire a correction flood to be used for multiplicative uniformity correction (*5*). Sources of inaccuracy are: (a) flood-source inhomogeneities, (b) mismatch of scatter conditions, (c) collimator nonuniformity, (d) nonuniformity of detector's point source sensitivity, (e) detector nonlinearity, (f) ADC nonlinearity, (g) random noise in the correction data.

A multiplicative uniformity correction compensates for (c) and (d). Colsher and Muehllehner (*9*) have shown that, with a noise-free correction matrix, multiplicative correction entirely removes the ring artifacts caused by (e) and (f), almost without resolution loss. We have observed that a mismatch between the scatter conditions in the flood and patient result in significant artifacts. In principle the nonuniformity of a detector that has perfect energy resolution would be independent of the scatter conditions. However, with detectors of finite energy resolution we have observed that, to reduce ring artifacts, head imaging requires 2.5 cm of scattering medium in

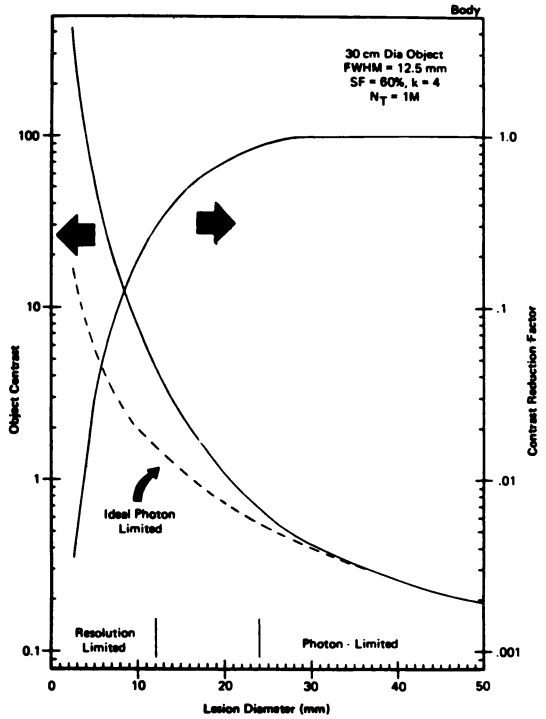

FIG. 4. SPECT lesion detectability and contrast reduction factor due to spatial resolution for sperical lesion in background of uniform activity, 30 cm in diameter.

front of and behind a liquid flood to match the scatter conditions, while body imaging requires 5 cm of such medium in front of and behind the flood. This procedure has the advantage of smoothing the inhomogeneities in the flood source. The remaining source of ring artifacts is the random noise in the flood matrix. This can be reduced only by acquiring sufficient counts in the correction flood.

The above correction procedure is not adequate for the center region because of the strong tendency of artifact amplification near the image center (*5*). According to our simulation, the noncircular orbit achieved by combination of rotational and translational motions shows a large decrease in the uniformity artifact at the image center (by a factor as much as 20) as well as a reduction by a factor of two in the off-center ring artifacts (*1*). This uniformity improvement would not occur if the noncircular orbit is achieved by changing only the rotation radius during the scan.

SPECT SYSTEM

The SPECT system used in our experiments was a gamma camera* mounted on an orbiting C-arm gantry and interfaced to a computer. This is an integrated SPECT system with array processor for fast reconstructions, 750K bytes of image memory, and a 27 Megabyte hard disk.

The camera has a 51 × 37 cm rectangular field of view. The rectangular detector is desirable in SPECT to permit use of the entire axial extent of the detector without truncation of the projection. The detector's spatial and energy resolutions were 4.1 mm FWHM and 11.7% FWHM. The detector has magnetic shields to reduce the angular variation of the detector uniformity. Measurement of regional sensitivity fluctuation with angle showed less than 1% variation (the statistical accuracy of the measurement) over the entire detector surface.

The SPECT computer controls both the rotational and translational motions, with feedback from the position and state of the SPECT system. The angle feedback is used by the reconstruction software to correct small ($\pm 1/16°$) angle errors during rotation, and for noncircular orbits the translation feedback is used to determine the translation amount to an accuracy of ±0.07 cm. Both translational and rotational motions were performed simultaneously, so there was no change in the total imaging time. All our images used 128 × 128 format, reconstructed from 120 equally spaced angular views of 128 × 128 matrix over 360°. The pixel size for acquisition and reconstruction was 2.92 mm square. The reconstructions used back-projection of filtered projections with a noniterative Chang's method for attenuation compensation. Reconstruction times per slice were 13 sec for 128 × 128 with 120 angles.

The location of the central ray as a function of angle was very important. Deviations of central ray locations among 120 projection views in our system had a maximum of 0.75 mm (¼ pixel) and an rms deviation of 0.5 mm (0.15 pixel). At each angular position it was systematic and reproducible, causing 6–7% level streak artifacts and 0.3 mm loss of resolution without central ray correction. The SPECT system compensates for this by imaging a line source at 120 angles over 360° and using the deviations to shift the projection central ray before back-projection. The method is accurate to 0.03 mm (0.01 pixel). This eliminates the resolution loss and reduces the level of streak artifact to below 1%. This procedure is automatic for all reconstructions. Calibration is performed on a biweekly basis. The central-ray correction did not have an axial dependence.

The axis of rotation was leveled to ±0.0005° accuracy. Measurements showed that it stayed level to this accuracy during rotation and translation along the AreaScan track.

All data were acquired with Tc-99m. The correction flood had 120 million counts in 128 × 128 image format. It was acquired with 15% energy window with 5 cm of scattering material in front of and behind the flood. A high resolution collimator was used for all measurements. No processing was performed on the correction matrix. We have seen no evidence of fluctuations in the correction matrix from detector drift over 2-wk periods.

EXPERIMENTAL RESULTS

We compared the circular and noncircular SPECT images for the following phantoms with Tc-99m source:

1. Line sources in water
2. Nonradioactive rods of 6,8,10,12,14, and 16 mm diameters in a uniform-activity cylinder 22 cm in diameter.
3. Jaszczak SPECT phantom
4. Alderson liver phantom with 1.7 cm and 2.3 cm nonradioactive spherical lesions.

An elliptical detector orbit was used for convenience. The first three measurements compared a circular orbit 40 cm in diameter with a 40 × 30 cm elliptical orbit, and the liver phantom compared a 42-cm circular orbit with a 42 × 31 cm elliptical. All orbit diameters were measured from the collimator face.

Resolution improvements. Bringing the detector 5 cm closer to the phantom would produce a 2.5 mm improvement in projection resolution, according to Fig. 2. We therefore expect horizontal resolution improvements of this order. We imaged five Tc-99m capillary tubes in a water bath 22 cm in diameter. The positions of the tubes and the resolutions measured in the horizontal direction are shown in Table 1. The resolution FWHM

TABLE 1. HORIZONTAL SPATIAL RESOLUTION MEASURED (FWHM IN MM)

Location (X, Y) IN CM	Elliptical orbit 30 cm × 40 cm	Circular orbit 40 cm × 40 cm
(0, 0)	12.0	14.2
(5, 0)	12.0	14.6
(7.5, 0)	11.9	14.3
(0, 5)	10.0	12.1
(0, 7.5)	9.1	10.5
		HR collimator

improvements ranged from 1.5 to 2.5 mm. The center-point resolution for the 40 cm circular orbit was 14.2 mm FWHM compared with 12.0 mm FWHM for the 40 × 30 cm ellipse. The FWTMs were 27.2 mm and 22.8 mm, respectively, with FWTM/FWHM ratios of 1.9.

Contrast and uniformity improvement. The resolution improvement will be reflected in the SPECT lesion contrast as higher-amplitude signals for small lesions and sharper edges for large lesions. For the contrast measurements we imaged nonradioactive 6, 8, 10, 12, 14, 16 mm in diameter, located at the same five positions within a uniform activity cylinder of 22 cm in diameter, as shown in Table 1. To obtain enough counts to measure contrast, and to test stringently the uniformity improvements, we integrated the reconstruction axially. The total counts/slice were 25 million with slices 4.38 cm thick.

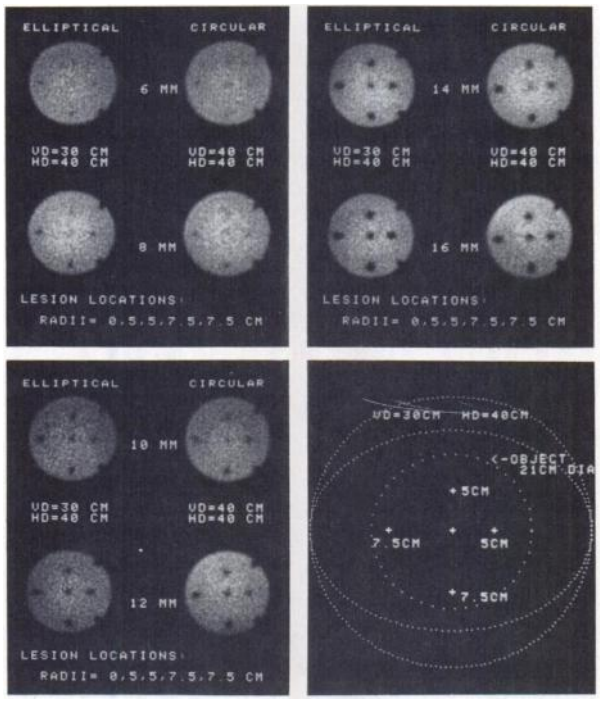

FIG. 5. Comparison of Tc-99m SPECT images of different-sized nonradioactive rods (diameters 6 mm to 16 mm at 2 mm increments), located at positions shown in Table 1, between elliptical orbit (VD = 30 cm, HD = 40 cm) and circular orbit (diam = 40 cm).

TABLE 2. MEASURED SPECT LESION CONTRAST IMPROVEMENTS IN ELLIPTICAL ORBIT OVER CIRCULAR ORBIT

Cylindrical lesion diameter (mm)	Contrast measured: Elliptical orbit 30 cm × 40 cm	Contrast measured: Circular orbit 40 cm × 40 cm	Relative contrast increase
6	0.20	<0.07	2.8
8	0.35	0.27	1.3
10	0.40	0.33	1.2
12	0.55	0.42	1.3
14	0.52	0.52	1.0

Lesions located at 7.5 cm from image center on short elliptical axis embedded in uniform activity 22 cm in diameter.

The reconstructions of the rods are shown in Fig. 5. With elliptical orbit the image shows four of the five 6 mm rods (top left) with no clear ring artifacts, whereas the circular orbit has a strong artifact at the center and only three of the five rods are visible. All five of the 8 mm rods are seen clearly with the elliptical orbit, whereas in the circular orbit they show in diffuse contrast with a ring artifact near the center, interfering with contrast at the center rod. The peripheral rods have visibly higher contrast and better shape definition with the elliptical orbit. For 10 mm and larger rods, both orbits allow detection of all five rods. However, the main difference between images from circular and elliptical orbits is again that the elliptical orbit shows better contrast, edge sharpness, and shape definition free of ring artifact, whereas the circular orbit tends to show with ring artifacts.

Quantitative measurements of contrast were made by inspecting a profile cutting through a lesion. The rod located at 7.5 cm vertical distance from the center was

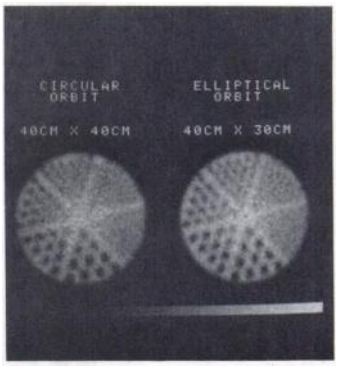

FIG. 6. Comparison of Tc-99m SPECT images of Jaszczak nonradioactive-rod phantom between elliptical (VD = 30 cm, HD = 40 cm) and circular orbit (diam = 40 cm). Rod diameters in each section are 4.9, 6.4, 7.9, 9.5, 11.1, and 12.7 mm, with rods, center-to-center distances twice rod diameter in each section. Note penetration of spoke detail to image center with elliptical orbit.

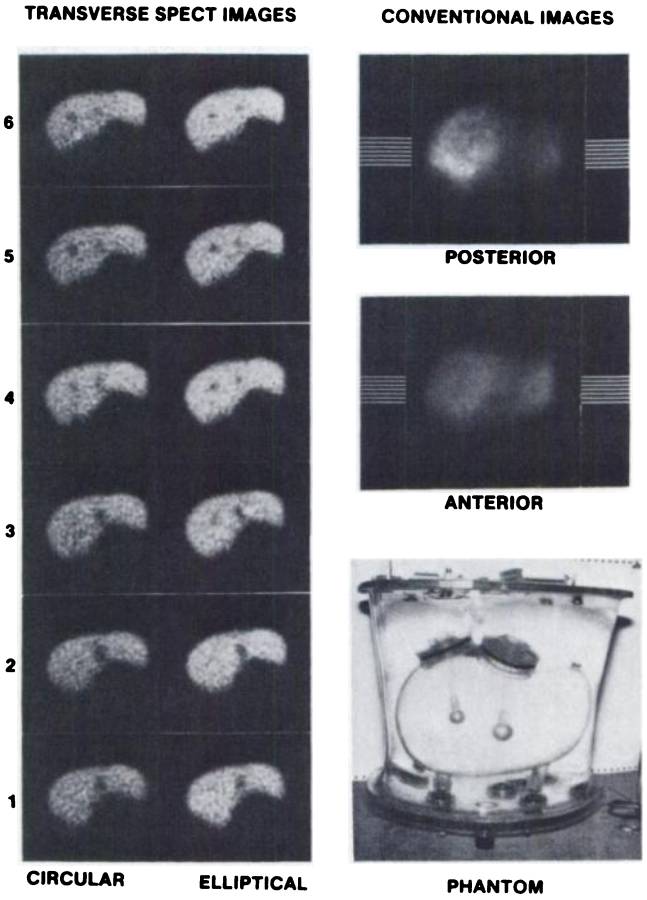

FIG. 7. Comparisons of Tc-99m SPECT slice images of Alderson liver phantom between elliptical (VD = 31 cm, HD = 40 cm) and circular (diam = 42 cm) orbits. Liver phantom had two nonradioactive-spherical lesions of diameters 1.7 cm and 2.3 cm each, as shown in phantom photograph. Six contiguous SPECT slices of 6.4 mm thickness cut through volume containing two lesions as shown in anterior and posterior conventional projection images.

chosen for profile inspection. Contrast measurements from the rods located at 5 cm radius and the center were unreliable because of the ring artifacts in the circular orbit. Average backgrounds near the peripheral rod were determined and the minimum count level within the area of the rod was measured. They were used to determine the contrast factors with varying rod size. The contrast improvements measured for different rod sizes are summarized in Table 2.

Jaszczak SPECT phantom. The Jaszczak phantom has six sectors of nonradioactive rods in a radioactive background 22 cm in diameter, with rod separation (center-to-center) twice the rod diameter. The rod diameters are 4.9, 6.4, 7.9, 9.5, 11.1, and 12.7 mm. The reconstructions are shown in Fig. 6. Both images have five million total counts. The elliptical orbit clearly shows improved contrast and resolution. The 7.9 mm sector (11.30 o'clock) is visible in the elliptical orbit, but not in the circular orbit, except the edge rods. The entire 9.5 mm sector is clearly seen with the elliptical orbit, but the circular orbit nearly loses the inner three rods. The 11.1 and 12.7 mm rods show better contrast and edge sharpness for the noncircular orbit. Notice the penetration of the spoke detail to the image center in the elliptical orbit.

Liver phantom. An Alderson liver phantom was imaged with 1.7 cm and 2.3 cm spherical nonradioactive lesions. Transverse section images are shown in Fig. 7, along with planar views and a phantom picture. The slice thickness was 6.4 mm with an average of 1.2 million counts/slice. The first slice was taken through the bottom of the 2.3-cm lesion. The second and fifth slices are cutting through the center of the 2.3-cm and 1.7-cm lesions, respectively. Both orbits clearly visualize the lesions, but the elliptical gives the lesions better contrast and shape definition. In the fifth slice the contrast of the 1.7 cm lesion is clearly better with the elliptical orbit. The nonradioactive foci in the fifth and sixth slices at the location of the 2.3 lesion are the images of the rod (9.6 mm diam) supporting 2.3 cm lesion sphere.It is visualized better with the elliptical orbit.

CONCLUSION

We have compared improvements of SPECT image quality between a 40 × 30 cm elliptical orbit and an equivalent circular orbit 40 cm in diameter. We have experimentally demonstrated improvements in resolution, contrast, edge definition, and uniformity. Also, we extracted quantitative information on the basic imaging parameters such as image resolution and lesion contrast from the SPECT image data. Resolution improvements (FWHM) were 1.5–2.5 mm. Contrast improvements were 20–30% for small lesions. The edges of large lesions

were better defined and crisper. The elliptical orbit showed no detectable uniformity artifacts and allowed reliable interpretation of the SPECT reconstruction at the center. All improvements were achieved without increasing the noise in the reconstruction, with no increase in processing time, and with no increase in the imaging time. In the clinical situation other sources of SPECT image degradation (such as organ motion) should be considered carefully.

FOOTNOTE

* Technicare Omega 500.

ACKNOWLEDGMENTS

We recognize Technicare Nuclear Engineering team for developing the Omega 500 ECT system. We thank Jim Janzo for fabricating special alignment equipment for this experiment, and Corby Sable for preparing phantoms. We acknowledge the encouragement and support of Messers. Arthur B. Braden, Donald Blake, and Robert Locker. Our special thanks go to Mrs. Vanessa Courie for preparing the manuscript.

REFERENCES

1. GOTTSCHALK SC, SALEM D: Effect of an elliptical orbit on SPECT resolution and image uniformity. In *Nuclear Medicine and Biology*. Reynaud C, Ed. Paris, Pergamon, Vol. I, 1982, pp 1026-1029
2. JASZCZAK RJ, WHITEHEAD FR, LIM CB, et al: Lesion detection with single-photon emission computed tomography (SPECT) compared with conventional imaging. *J Nucl Med* 23:97-102, 1982
3. LIM CB, HAN KS, HAWMAN EG, et al: Image noise, resolution, and lesion detectability in single photon emission CT. *IEEE Trans Nucl Sci* NS-29:500-505, 1982
4. JASZCZAK RJ, COLEMAN RE, WHITEHEAD FR: Physical factors affecting quantitative measurements using camera-based single photon emission computed tomography (SPECT). *IEEE Trans Nucl Sci* NS-28:69-80, 1981
5. ROGERS WL, CLINTHORNE NH, HARKNESS BA, et al: Field flood requirements for emission computed tomography with an anger camera. *J Nucl Med* 23:162-168, 1982
6. CHESLER DA, RIEDERER SJ, PELC NJ: Noise due to photon counting statistics in computed x-ray tomography. *J Comput Assist Tomogr* 1:64-74, 1977
7. BUDINGER TF, GULLBERG GT, HUESMAN RH: Emission computed tomography, In *Image Reconstruction from Projection, Implementation and Application, Vol. 32: Topics in Applied Physics*. Herman GT, Ed. New York, Springer-Verlag, 1979 Chap. 5, pp 147-246
8. LIM CB, CHANG LT, JASZCZAK RJ: Performance analysis of three camera configurations for single photon emission computed tomography. *IEEE Trans Nucl Sci* NS-27:559-568, 1980
9. COLSHER JG, MUELLEHNER G: *Spatial Linearity Requirements for Rotating Gamma Camera SPECT. Nuclear Medicine and Biology*. Reynaud C, Ed. Paris, Pergamon, Vol. 1: 1982 pp 1022-1025
10. CHANG LT: A method for attenuation correction in radionuclide computed tomography. *IEEE Trans Nucl Sci* NS-25:638-643, 1978